ChemEurJ

Research Article
doi.org/10.1002/chem.202501515

Chemistry Europe
European Chemical Societies Publishing

www.chemeurj.org

$Pd[B(S_2O_7)_2]_2$ and $Pd[B(SO_4)(S_2O_7)]_2$: Two Borosulfates with Pd^{2+} in Octahedral and One with Pd^{2+} in Square Planar Oxygen Coordination

Stefan Sutorius,[a] David Patrun,[a] Arthur Edelmann,[a] Lars Schumacher,[b] Rainer Pöttgen,*[b] Markus Suta,*[c] and Jörn Bruns*[a]

The reaction of elemental palladium with B_2O_3 and SO_3 at elevated temperature results in the formation of blue crystals of $Pd[B(S_2O_7)_2]_2$. Dependent on the reaction conditions, the compound crystallizes in two different polymorphs obtained as bulk samples. In both structures the Pd^{2+} cations are coordinated by six oxygen atoms in form of an almost perfect octahedron. All oxygen atoms belong to the borosulfate anions $[B(S_2O_7)_2]^-$ and link via Pd^{2+} cations to an extended network structure. Within the uncommon octahedral oxygen coordination, the Pd^{2+} cations reveal a d^8 high-spin configuration, which leads to paramagnetism. Occasionally, red crystals are formed during the reaction next to the major fraction of blue crystals of $Pd[B(S_2O_7)_2]_2$. Single crystal X-ray structure analysis on the red crystals reveals the sum formula $Pd[B(SO_4)(S_2O_7)]_2$ with Pd^{2+} in square-planar coordination.

1. Introduction

Since the publication of the first crystallographically characterized borosulfate $K_5[B(SO_4)_4]$ the number of new representatives has continuously risen.[1] At the time of the present work, classical and unconventional borosulfates can be differentiated.[2] The classical borosulfates exclusively feature anions with alternatingly vertex-connected (BO_4)- and (SO_4)-tetrahedra, whereas unconventional borosulfates might also contain fragments with connections of at least two (BO_4)— or two (SO_4)—tetrahedra forming B—O—B or S—O—S bonds, respectively.[2] Apart from some exceptions, borosulfates are typically charge-compensated by mono-, di-, or trivalent-cations.[2] Besides their unique structural features, borosulfates have attracted interest as, for example, nonlinear optical (NLO) materials,[3] as solid acid polyelectrolytes[4] or as potential hosts leading to uncommon luminescence properties.[5] However, a major focus so far has been on the synthesis and characterization of new borosulfates since the compound class is still quite new. These studies led to many impressive results. From the field of classical borosulfates, $Mg_3[H_2O{\rightarrow}B(SO_4)_3]_2$ may serve as illustrative example.[6] The latter exhibits a *Lewis*-acid-base adduct of water to a $[B(SO_4)_3]^{3-}$ moiety. From the field of unconventional borosulfates, we recently presented the strontium compound $Sr[B_3O(SO_4)_4(SO_4H)]$, exhibiting an anionic substructure with not only two but even three (BO_4) tetrahedra connected via one common vertex.[7] This unique representative can be obtained from reactions with a special setup to provide the (SO_4)-source. In contrast, borosulfates with the connection of two (SO_4)-tetrahedra via one common vertex are able to stabilize the polycation $(I_4)^{2+}$ in the compound $(I_4)[B(S_2O_7)_2]_2$.[8] Thus far, it was known that the stabilization of $(I_4)^{2+}$ cations is successful when suitable starting materials react with sufficiently strong oxidizing agents under the formation of weakly coordinating anions during the reactions. In the aforementioned case SO_3 acts as strong oxidizer and the $[B(S_2O_7)_2]^-$ anions must be weakly coordinating. The extreme and unusual conditions are most likely also the reason for the formation of the cluster-like and wave-like Au-Cl heteropolycations in the compounds $[Au_3Cl_4][B(S_2O_7)_2]$ and $[Au_2Cl_4][B(S_2O_7)_2](SO_3)$.[9]

With the aim to stabilize additional unconventional noble metal species, we now focused on the element palladium. In solid-state compounds +2 and +4 are the predominant oxidation states, whereas the latter is quite rare. This is insightful based on the fact that it is not sufficient to react Pd^{4+} compounds with the strong oxidizer SO_3 to obtain compounds with tetravalent palladium. Pd^{4+} can, however, be stabilized upon addition of XeF_2 to the reaction mixture.[10] In contrast, oxidic and oxoanionic compounds of divalent palladium are not rare. Most of these compounds exhibit almost perfect square planar

[a] S. Sutorius, D. Patrun, A. Edelmann, PD Dr. J. Bruns
Institut für Anorganische und Materialchemie, Universität zu Köln, Greinstraße 6, 50939 Cologne, Germany
E-mail: j.bruns@uni-koeln.de

[b] L. Schumacher, Prof. Dr. R. Pöttgen
Institut für Anorganische und Analytische Chemie, Universität Münster, Corrensstraße 30, 48149 Münster, Germany
E-mail: pottgen@uni-muenster.de

[c] Jun. Prof. Dr. M. Suta
Inorganic Photoactive Materials, Institute of Bioinorganic Chemistry, Heinrich Heine University Düsseldorf, Universitätsstraße 1, 40225 Düsseldorf, Germany
E-mail: markus.suta@hhu.de

Supporting information for this article is available on the WWW under https://doi.org/10.1002/chem.202501515

(PdO_4)-moieties, which is a textbook example of the electronic stabilization of a $4d^8$ ion in a strong ligand field due to d_{z^2-s} mixing in a square-planar coordination geometry with consequent diamagnetism. Illustrative examples are the binary oxide PdO,[11] the nitrate and methanesulfonate $Pd(NO_3)_2$ and $Pd(CH_3SO_3)_2$[12] as well as the sulfate $Pd(SO_4)$.[13] Rarer are species with Pd^{2+} in an octahedral ligand field, which is most commonly known for the respective fluorides.[14] However, if the network is very rigid, oxygen atoms can also serve as ligands for octahedrally coordinated Pd^{2+} cations, like in the oxides Ca_2PdWO_6 and $PdAs_2O_6$.[15,16] In the polyoxometallates $[Pd_{12}(AsPh)_8O_{32}]^{6-}$ and $[Pd_{13}Se_8O_{32}]^{6-}$ is one of the 13 divalent palladium cations in octahedral or even cubic environment.[17] The oxoanionic species palladium disulfate $Pd(S_2O_7)$ and palladium hydrogendisulfate $Pd(HS_2O_7)_2$ were obtained from reactions in SO_3 and oleum, respectively.[18,19] Both compounds crystallize as blue or purple-blue crystals and exhibit an almost ideal octahedral oxygen coordination around the central Pd^{2+} cations. In accordance with that coordination geometry, bulk samples of $Pd(S_2O_7)$ and $Pd(HS_2O_7)_2$ are paramagnetic and even exhibit ferromagnetic ordering at low temperatures.[18,19]

2. Results and Discussion

In the course of our studies on borosulfates, we have now come across two polymorphs of $Pd[B(S_2O_7)_2]_2$. These new borosulfates were obtained in form of blue crystals (Figure 1) from solvothermal reactions between elemental palladium, boron oxide, and SO_3.

Hitherto, we were not able to crystallize $Pd[B(S_2O_7)_2]_2$ from oleum, despite that fact that a compound with the same anion, namely $Ag[B(S_2O_7)_2]$, has been obtained from a solvothermal reaction in oleum (65% SO_3).[20] The crystals are very sensitive to moisture and rapidly decompose if not handled under strictly inert conditions.

Both compounds contain Pd^{2+} in an octahedral coordination geometry surrounded by oxygen atoms (Figure 2 and Figure 5) stemming from $[B(S_2O_7)_2]^-$ anions. An octahedral oxygen-based coordination is quite uncommon for divalent palladium cations. Accordingly, both representatives are, among few other compounds known in literature, rare examples for such a special arrangement and obviously borosulfate anions are able to stabilize Pd^{2+} even in this special coordination geometry, which must be related to their weak coordination behavior sufficiently weakening the ligand field that makes a stabilization of the square-planar coordination geometry not feasible.

Polymorph I (in the following denoted as $Pd[B(S_2O_7)_2]_2$-I) crystallizes in the monoclinic space group $P2_1/c$ (no. 14) with two formula units per cell. The structure is built up by Pd^{2+} cations (special Wyckoff position 2*c*) and *bis*-disulfatoborate anions $[B(S_2O_7)_2]^-$ (Figure 2).

The $[B(S_2O_7)_2]^-$ anions are constituted by a central boron atom coordinated by two bidentate chelating $(S_2O_7)^-$subunits. Each of the $[B(S_2O_7)_2]^-$ anions bridge three Pd^{2+} cations in a monodentate fashion, respectively (Figure 3).

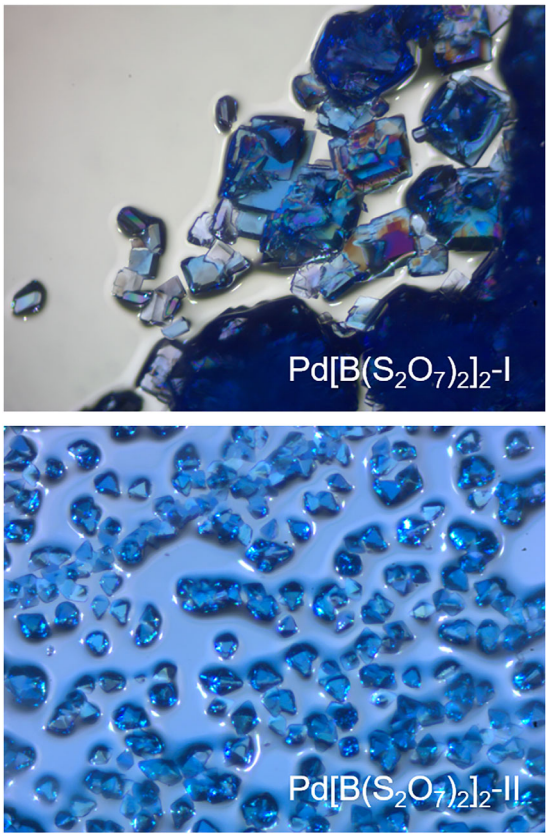

Figure 1. Blue crystals of $Pd[B(S_2O_7)_2]_2$-I (top) and $Pd[B(S_2O_7)_2]_2$-II (bottom) under a polarization microscope. The crystals decompose immediately even under protecting oil.

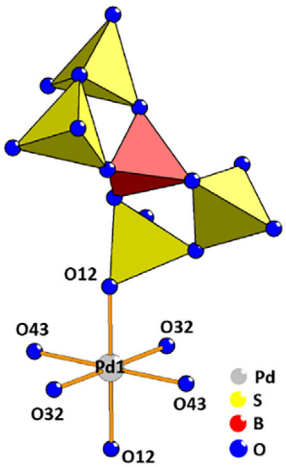

Figure 2. Octahedral oxygen coordination around the central Pd^{2+} cations in the structure of $Pd[B(S_2O_7)_2]_2$-I. Selected bond lengths [Å]: Pd1–O12 2.163(2), Pd1–O32 2.204(2), Pd1–O43 2.239(2).

Thus, a 3D network structure is formed (Figure 4). Each Pd^{2+} cation is coordinated by six $[B(S_2O_7)_2]^-$ anions. The B—O bonds have an average length of 1.46 Å, while the terminal S—O bond lengths are 1.41 Å. The bond lengths of the S—O—S bridge are 1.62 Å, the S—O bond lengths of the oxygen atoms coordinating to Pd^{2+} are 1.43 Å and the S—O bond lengths of the oxygen atoms coordinating to boron are determined to 1.52 Å (see

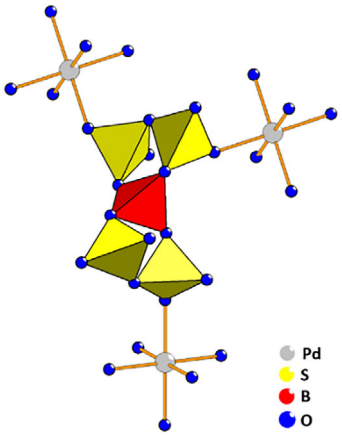

Figure 3. Coordination of the $[B(S_2O_7)_2]^-$ anion in the structure of $Pd[B(S_2O_7)_2]_2$-I.

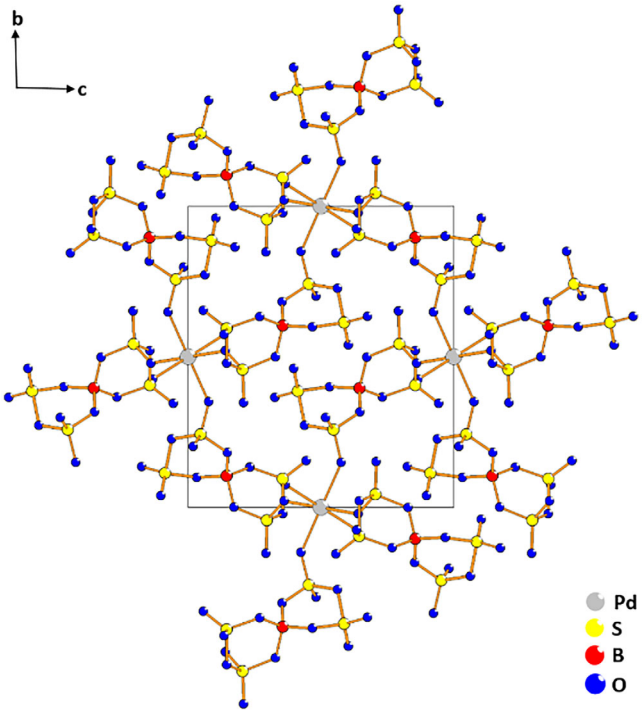

Figure 4. Crystal structure of $Pd[B(S_2O_7)_2]_2$-I in projection onto the *bc*-plane.

Table 1). These values are in good agreement with the findings for $Ag[B(S_2O_7)_2]$.[20]

The Pd—O bond lengths reveal no significant elongation. Thus, there is no hint for a Jahn-Teller distortion, as would be expected for an octahedral d^8 configuration with an orbitally singly degenerate $^3A_{2g}(^3F)$ ground state. The Pd—O bond lengths fall in the narrow range of 2.163(2) to 2.239(2) Å. The largest deviation from the ideal angles of 90° and 180° within the octahedron occurs between O32 and O43 and amounts to 7.6°. The latter is a bit higher than found for $Pd(S_2O_7)$ and $Pd(HS_2O_7)_2$ with values of 4.8° and 4°, respectively.[18,19] The Pd—O bond lengths of $Pd(S_2O_7)$ and $Pd(HS_2O_7)_2$ are somewhat more asymmetric with values ranging from 2.175(1) to 2.239(1) Å and 2.189(1) to 2.208(1) Å, respectively.[18,19]

Table 1. Average bond lengths in the three structures. (bold letters are the examined bonds).

Bond	Average bond lenghth of $Pd[B(S_2O_7)_2]_2$-I [Å]	Average bond lenghth of $Pd[B(S_2O_7)_2]_2$-II [Å]	Average bond lenghth of $Pd[B(SO_4)(S_2O_7)]_2$ [Å]
Pd—O	2.20	2.20	2.02
S—O—Pd	1.43	1.44	1.47
B—O—S	1.46	1.47	1.47
S—O—B	1.52	1.52	1.52
S—O—S	1.62	1.63	1.63
S—$O_{terminal}$	1.41	1.41	1.41

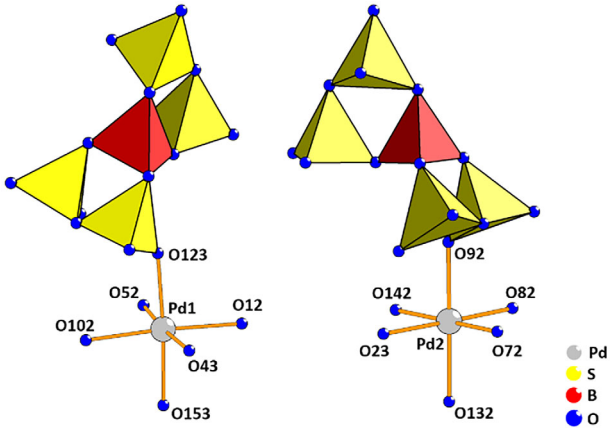

Figure 5. Octahedral oxygen coordination around the central Pd^{2+} cations in the structure of $Pd[B(S_2O_7)_2]_2$-II. Selected bond lengths [Å]: Pd1–O12 2.210(3), Pd1–O102 2.204(4), Pd1–O123 2.195(3), Pd1–O153 2.184(3), Pd1–O43 2.200(3), Pd1–O52 2.187(3), Pd2–O132 2.199(3), Pd2–O142 2.191(4), Pd2–O23 2.196(3), Pd2–O72 2.198(4), Pd2–O82 2.208(3), Pd2–O92 2.202(3).

The second polymorph (denoted as $Pd[B(S_2O_7)_2]_2$-II in the following) crystallizes in the tetragonal space group $P4_1$ (no. 76). This polymorph reveals two crystallographically independent Pd^{2+} cations (Wyckoff positions 4*a*, Figure 5) and four different $[B(S_2O_7)_2]^-$ anions (Figure 6).

Like in polymorph I, all Pd^{2+} cations are coordinated by six $[B(S_2O_7)_2]^-$ anions in a monodentate fashion in polymorph II. The B—O bonds have an average length of 1.47 Å and the terminal S—O bond lengths show no evidence for disorder or protonation (for detailed values, see Table S9 in the SI).

Each Pd^{2+} cation is coordinated by six oxygen atoms in form of slightly distorted octahedra. The Pd—O bond lengths fall in the narrow range of 2.184(3) to 2.210(3) Å. Again, there is no hint for Jahn-Teller distortion. Each of the four crystallographically independent $[B(S_2O_7)_2]^-$ anions in polymorph II are coordinated by three Pd^{2+} cations and thus the structure forms a 3D network.

Both compounds crystallize from reactions with very similar reaction conditions (see experimental section). However, the described reactions do not always lead to phase pure samples of the desired products, most likely due to small temperature differences within the oven. We assume that even small temperature differences resulting from different positions in the tube furnace are sufficient to significantly influence the reaction.

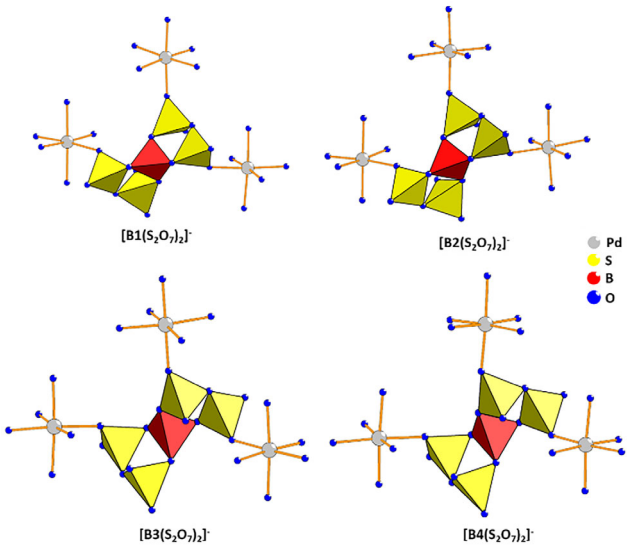

Figure 6. Coordination of the four crystallographically independent $[B(S_2O_7)_2]^-$ anion in the structure of $Pd[B(S_2O_7)_2]_2$-II.

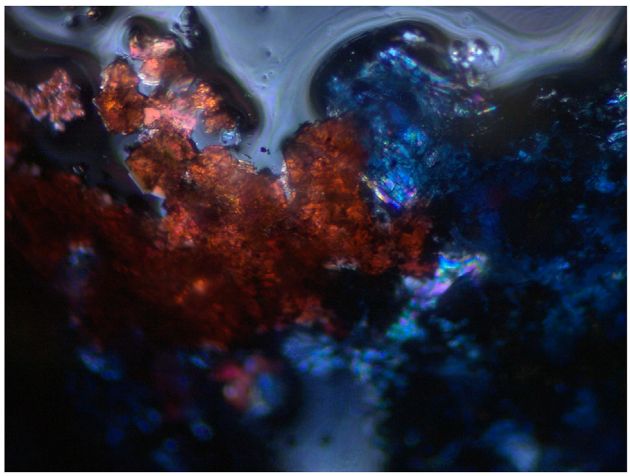

Figure 7. Crystals of red $Pd[B(SO_4)(S_2O_7)]_2$ under a polarization microscope.

Furthermore, occasionally red crystals of a compound with the sum formula $Pd[B(SO_4)(S_2O_7)]_2$ can be isolated next to the blue crystals in the glass ampoule after cooling to room temperature (Figure 7). However, it was so far not possible to isolate a phase pure bulk sample of the red species.

As expected from the color of the crystals, in this compound Pd^{2+} is coordinated in a square-planar fashion by four oxygen atoms. The latter belong to borosulfate anions (Figure 8).

The Pd–O bond lengths in that compound fall in the narrow range of 1.996(2) to 2.038(3) Å, which is in good agreement with values found for square-planarly coordinated Pd^{2+} in the anion $[Pd(S_4O_{13})_2]^{2-}$.[21] The borosulfate anions reveal a chain-like arrangement with central boron atoms bridged in an alternating fashion by $(S_2O_7)-$ and $(SO_4)-$units and are thus similar to the structure found, for example, for $Cs[B(SO_4)(S_2O_7)]$ and $H[B(SO_4)(S_2O_7)]$.[22]

The anionic chains in $Pd[B(SO_4)(S_2O_7)]_2$ run parallel to the *c* axis (Figure 9) and are packed in a layer-like arrangement with Pd^{2+} cations (Figure 10).

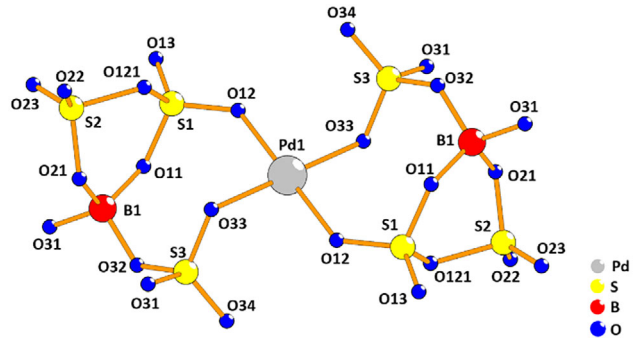

Figure 8. Square planar oxygen coordination around the central Pd^{2+} cations in the structure of red $Pd[B(SO_4)(S_2O_7)]_2$. Selected bond lengths [Å]: Pd1—O12 2.038(3), Pd1—O33 1.996(2).

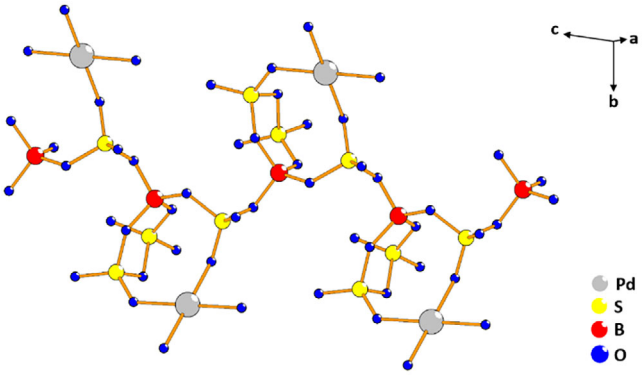

Figure 9. Coordination of the borosulfate anion in the structure of red $Pd[B(SO_4)(S_2O_7)]_2$.

According to powder X-ray diffraction $Pd[B(S_2O_7)_2]_2$-I and $Pd[B(S_2O_7)_2]_2$-II have been obtained as pure phases, respectively (Figure 11).

Magnetic measurements reveal that both samples exhibit Curie-Weiss behavior with no magnetic ordering in the measured temperature range (Figures 12 and 13). Their effective magnetic moments were calculated from Curie-Weiss fits using the data from the temperature range of 100 to 300 K. The experimental moments, the Weiss constants, and the values of the highest magnetization are listed in Table 2.

The octahedrally surrounded Pd^{2+} ion ($4d^8$) is expected to exhibit a spin-only magnetic moment of 2.83 μ_B.[23] This behavior was observed in $Pd(S_2O_7)$[18] with an effective moment of μ_{eff} = 2.89(1) μ_B Pd atom^{-1}. In the two polymorphs of $Pd[B(S_2O_7)_2]_2$, however, the magnetic moments are slightly increased (Table 2). This is most likely due to stronger spin-orbit coupling and already indicates an even weaker coordination of the surrounding $[B(S_2O_7)_2]^-$ ligands compared to the $[S_2O_7]^{2-}$ ligands and a consequent insufficient orbital quenching by the ligand field.[23]

Similarly increased moments have been observed for $CsPd_2F_5$ (μ_{exp} = 3.07 μ_B Pd atom^{-1})[14f] and the $PdTF_6$ phases (T = Zr, Pd, Sn, Hf, Pt) with a range from 2.88 to 3.10 μ_B Pd atom^{-1}.[24] The very small Weiss constants close to 0 K indicate negligible interactions within the paramagnetic range (see Table 2).

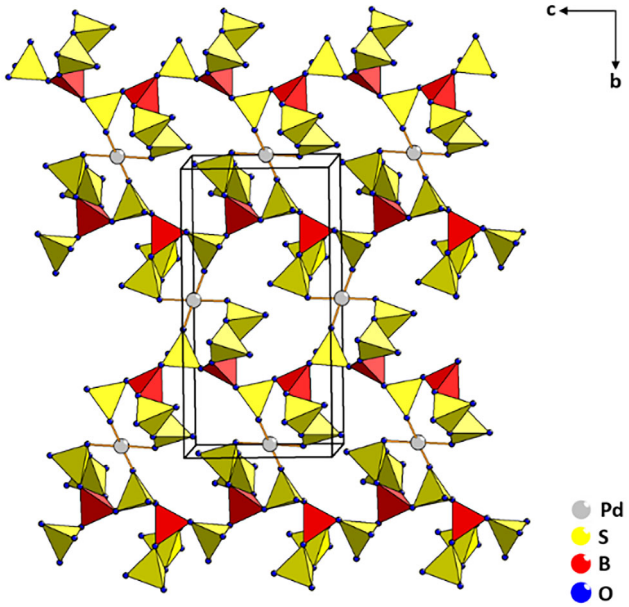

Figure 10. Crystal structure of red $Pd[B(SO_4)(S_2O_7)]_2$ in view approximately onto the *bc*-plane.

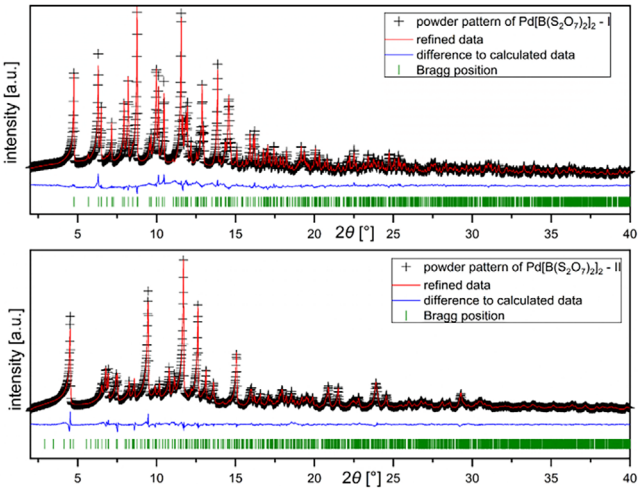

Figure 11. (top) Rietveld refinement plot of $Pd[B(S_2O_7)_2]_2$-I. The following profile *R*-factors were received: R_{exp} = 1.23%, R_{wp} = 5.08%, R_p = 3.98%, GOF = 4.14. (bottom) Rietveld refinement plot of $Pd[B(S_2O_7)_2]_2$-II. The ollowing profile *R*-factors were received: R_{exp} = 1.63%, R_{wp} = 3.89%, R_p = 2.92%, GOF = 2.39.

The saturation magnetization values at 2 K and 90 kOe are well below the theoretical maximum (Figures 12 and 13, bottom). Much higher field strengths are needed to achieve full parallel spin alignment.

Another feature of the weak coordination of the $[B(S_2O_7)_2]^-$ anion is the striking blue color of crystals of $Pd[B(S_2O_7)_2]_2$ similar to $Pd(S_2O_7)_2$.[18] There are only very few other examples with octahedrally coordinated Pd^{2+} such as $LiPdAlF_6$ or $PdZrF_6$[14e] that are also reported having such a deep blue color. In fact, other solid crystalline compounds with octahedrally coordinated Pd^{2+} such as $KPdF_3$[14c,i] with a perovskite structure or Pd^{2+} incorporated into $CsNiCl_3$—type hexagonal

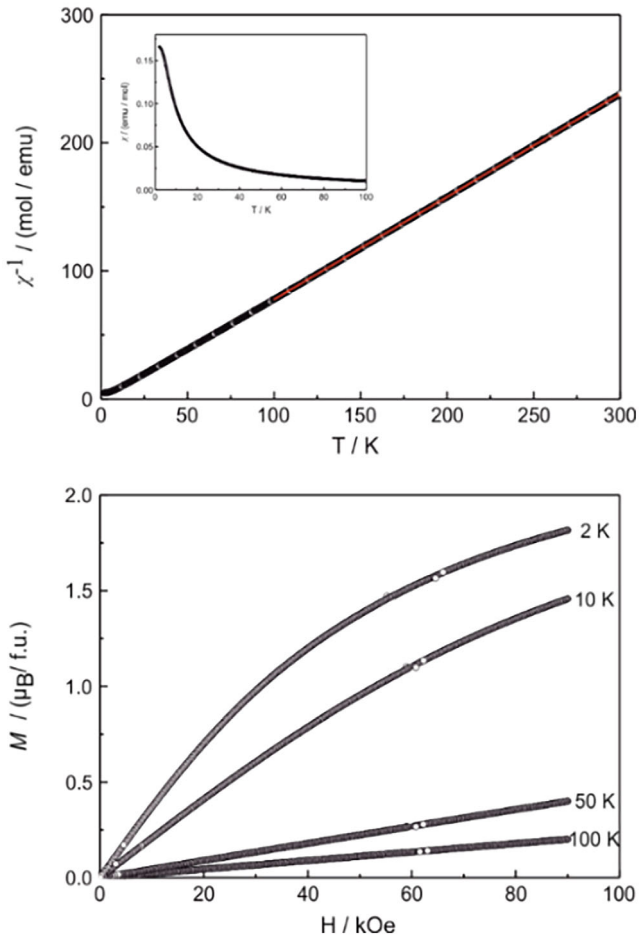

Figure 12. Magnetic data of $Pd[B(S_2O_7)_2]_2$-I: Inverse magnetic susceptibility measured with an applied external magnetic field of 10 kOe (top); zero field cooled/field cooled (ZFC/FC) measurement with an applied magnetic field of 100 Oe (inset); magnetization isotherms recorded at 2, 10, 50, and 100 K.

$CsMgCl_3$ containing trigonally distorted $[PdCl_6]^{4-}$ octahedra are also known.[25] Single crystals of those compounds were, however, found to have a deep red or tint violet ("amethyst-like") color, respectively. $CsMgCl_3$:Pd^{2+} serves as a useful example here. Its absorption spectrum in the visible range is dominated by two broad bands due to the $^3T_{2(g)}(^3F) \leftarrow {}^3A_{2(g)}(^3F)$ and $^3T_{1(g)}(^3F) \leftarrow {}^3A_{2(g)}(^3F)$ local transitions for a d^8 ion in an octahedral coordination environment. According to the Tanabe-Sugano diagram for an octahedrally coordinated d^8 ion (see Figure S3 in the Supporting Information), these two transitions must be at rather low energies indicating a weak ligand field since otherwise, a square-planar coordination would be electronically more favorable. While the low-intensity $^3T_{2(g)}(^3F) \leftarrow {}^3A_{2(g)}(^3F)$ is located in the deep red or NIR range and therefore expectedly gives rise to a weak cyan body color, the more intense $^3T_{1(g)}(^3F) \leftarrow {}^3A_{2(g)}(^3F)$ transition in the absorption spectrum of $CsMgCl_3$:Pd^{2+} peaks at around 530 nm is located in the green spectral range and thus explains the deep red color of the crystals.[25] Together, this leads to a tint violet color of the crystals in many compounds with octahedrally coordinated Pd^{2+}.

In first approximation, two factors determine the energy of excited many-electron states of transition metal ions in an

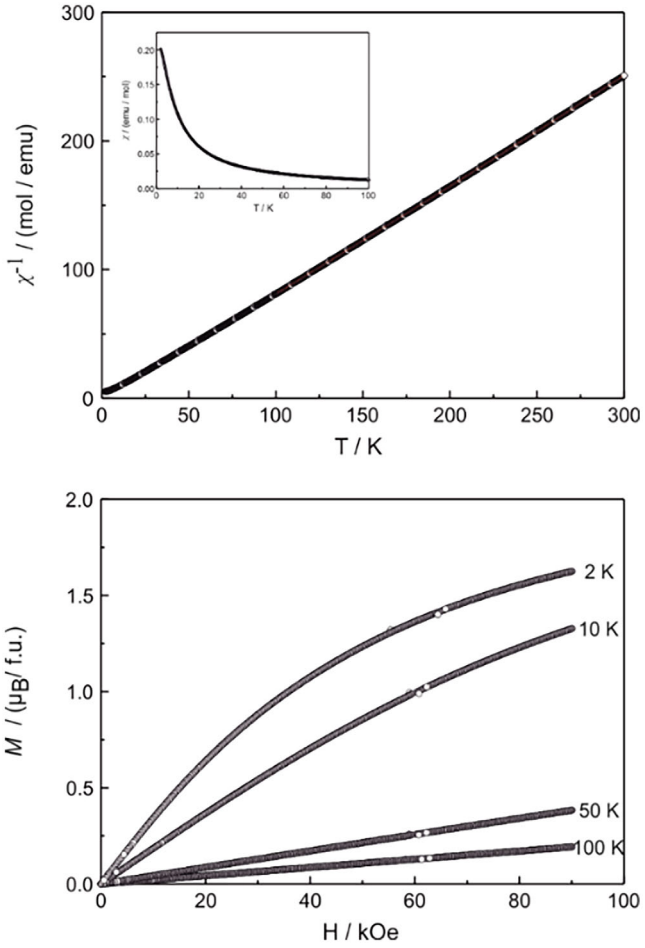

Figure 13. Magnetic data of $Pd[B(S_2O_7)_2]_2$-II: Inverse magnetic susceptibility measured with an applied external magnetic field of 10 kOe (top); zero field cooled/field cooled (ZFC/FC) measurement with an applied magnetic field of 100 Oe (inset); magnetization isotherms recorded at 2, 10, 50, and 100 K.

octahedral ligand field. On the one hand, the degree of ligand field strength plays a crucial role as broad-band excitations arise due to excitation of an electron from the rather nonbonding t_{2g}-transforming to the more antibonding e_g-transforming d orbitals. However, the energy of the electronic terms of the free ion is also dependent on the degree of mutual electron repulsion, which is usually parametrized by the Racah parameters for the transition metal ions. The electron repulsion decreases for a higher degree of delocalization of electron density along the metal–ligand bond (nephelauxetic effect). Based on our previous findings on octahedrally coordinated Mn^{2+} in a borosulfate,[5] we can conclude that these ligands are not only weakly coordinating but also tend to barely withdraw electron density from the transition metal ion. Thus, both $[S_2O_7]^{2-}$ and $[B(S_2O_7)_2]^-$ ligands lead to a weak ligand field (low *Dq*) and a limited degree of delocalization (high Racah parameter *B*). The lack of any cooperative magnetic effects relying on exchange interactions (see Figures 12 and 13) and the slightly enhanced effective magnetic moment compared to the spin-only moment due to a lacking orbital quenching (see Table 2) are clear experimental realizations of the nature of that chemical bonding situation.

Table 2. Magnetic properties of the two polymorphs of $Pd[B(S_2O_7)_2]_2$: μ_{exp} experimental magnetic moment; μ_{eff} effective magnetic moment; θ_P (K) paramagnetic Curie temperature; μ_{sat} experimental saturation magnetization; 2 *S* theoretical saturation magnetization.[18]

Compound	μ_{exp} [μ_B]	μ_{eff} [μ_B]	θ_P [K]	μ_{sat} [μ_B per Pd^{2+}]	2 *S* [μ_B per f. u.]
$Pd[B(S_2O_7)_2]_2$-I	3.18(1)	2.83	+1.9(1)	1.82(1) (2 K, 90 kOe)	2
$Pd[B(S_2O_7)_2]_2$-II	3.16(1)	2.83	−0.1(1)	1.63(1) (2 K, 90 kOe)	2

In the case of $Pd[B(S_2O_7)_2]_2$ or $Pd(S_2O_7)$,[18] the energies of the two excited $^3T_{2(g)}(^3F)$ and $^3T_{1(g)}(^3F)$ states should be expectedly slightly lower than in the case of the previously described cases of fluorides and chlorides. The $^3T_{1(g)}(^3F) \leftarrow {}^3A_{2(g)}(^3F)$ transition (describing an excitation of an electron from a t_{2g-} to an e_{g-}transforming d orbital) will then be rather located in the lower energetic yellowish or orange range thus leading to a blue body color of the crystals $Pd[B(S_2O_7)_2]_2$. Once the degree of electron delocalization is enhanced (which lowers the Racah interelectronic repulsion parameter *B*) and the ligand field becomes slightly stronger, the perceived color of compounds with octahedrally coordinated Pd^{2+} ions should expectedly shift toward the violet and then red accompanied by the observation of magnetic ordering at gradually higher temperatures. This is in line with the observations in, for example, $Pd(HS_2O_7)_2$ (violet, ferromagnetic with $T_C \approx 8$ K),[19] $PdAs_2O_6$ (violet, antiferromagnetic with $T_N \approx 150$ K),[16] or rutile-type PdF_2 (violet, antiferromagnetic with $T_N \approx 225$ K).[14a,b,26] It should be noted that the structure types and the connectivity between the Pd^{2+} ions will be similarly relevant for the magnetic ordering effects. This might explain why still no magnetic ordering has been detected for both modifications of $Pd[B(S_2O_7)_2]_2$ down to 2 K (closest Pd—Pd distances of around 750 pm) compared to $Pd(S_2O_7)$ ($T_C = 11.7$ K, closest Pd—Pd distances of around 500 pm) despite similar colors.[18] Future considerations by means of the angular overlap model and inclusion of second coordination sphere effects may be insightful to understand the electronic situation of the octahedrally coordinated Pd^{2+} ions in more detail.[27]

3. Conclusion

We demonstrated the syntheses of three new palladium borosulfates from the reactions of elemental palladium with B_2O_3 and SO_3 at elevated temperature. Two polymorphs with the sum formula $Pd[B(S_2O_7)_2]_2$ were obtained as blue crystals. Both structures exhibit Pd^{2+} cations in octahedral oxygen coordination, the latter originating from borosulfate anions. Accordingly, Pd^{2+} reveals a d^8 high-spin configuration and, thus leads to paramagnetism. Occasionally, red crystals could be obtained next to the blue crystals of $Pd[B(S_2O_7)_2]_2$ and were investigated via single crystal X-ray structure analysis. The latter revealed the sum formula $Pd[B(SO_4)(S_2O_7)]_2$ for the investigated species, with Pd^{2+} cations residing in square-planar oxygen coordination.

4. Experimental Section

CAUTION!!! SO_3 needs careful handling since it is a strong oxidizer. After the ampoule is closed it might be under remarkable pressure, even after the reaction. Before opening the ampoule should be cooled with liquid nitrogen.

Synthesis of the Pd[B(S$_2$O$_7$)$_2$]$_2$ polymorphs: Pd (50 mg, Heraeus, Germany) and B_2O_3 (40 mg for Pd[B(S_2O_7)$_2$]$_2$-I, 50 mg for Pd[B(S_2O_7)$_2$]$_2$-II, Alfa Aesar, Karlsruhe, Germany, 99 %) were ground together and transferred into a thick-walled glass ampoule (l = 200 mm, ø = 16 mm, thickness of the tube wall = 1.8 mm). The ampoule was attached to a specially constructed apparatus for the synthesis, handling, and application of SO_3 under inert atmosphere. Therefore, oleum (20% SO_3, Sigma-Aldrich, Darmstadt, Germany) was added carefully to an excessive amount of P_4O_{10} (97%, Merck, Darmstadt). The generated SO_3 can be transferred to the gaseous phase by increasing the temperature of the oleum/SO_3/P_4O_{10} mixture with an oil bath to 130 °C. The pressure within the apparatus is constantly monitored by a Teflon-lined manometer, which is attached above the dropping funnel. SO_3 condenses into a burette. The burette is part of the specially designed apparatus and accessible after opening a Teflon-lined valve. The ampoule containing the solid starting material is attached directly underneath the burette. Liquid SO_3 can be titrated into the ampoule. 0.4 mL SO_3 were needed for the phase-pure synthesis of Pd[B(S_2O_7)$_2$]$_2$-I and Pd[B(S_2O_7)$_2$]$_2$-II. The ampoule was torch sealed and placed in a tube furnace, which was heated up to 383 K over a period of 24 hours. The temperature was kept constant for 48 hours and reduced to 298 K within 90 hours. Following the initial reaction, the mother liquor was separated from the blue crystals via decantation. The SO_3-containing side of the ampoule was cooled with liquid nitrogen and several crystals were transferred into inert oil (Perfluoropolyalkylether AB128333, ABCR, Karlsruhe, Germany) directly after cracking the ampoule open (Figure 1). According to powder X-ray diffraction, both products could be synthesized as pure phases (see Figure 11). However, the previously described reactions do not reproducibly lead to phase pure samples of the desired products, most likely due to small temperature differences within the furnace.

X-ray crystallography: The crystals were handled in a glovebox and transferred under protective oil. A suitable crystal for single crystal X-ray diffraction was prepared under a polarization microscope. Mounted onto a loop (MicroMounts, MiTeGen LLC, New York, USA), the crystal was placed inside the diffractometer (Bruker D8 Venture, Karlsruhe, Germany) into a stream of cold nitrogen (100 K). After determining the unit cell, the reflection intensities were collected.

Pd[B(S_2O_7)$_2$]$_2$-I: blue blocks (0.03 × 0.10 × 0.15 mm), monoclinic, $P2_1/c$, $Z = 2$, $a = 7.2686(4)$ Å, $b = 12.7802(7)$ Å, $c = 11.4930(7)$ Å, $\beta = 101.343(2)°$, $V = 1046.8(1)$ Å^3, $\rho = 2.64$ g·cm^{-3}, $2\theta_{max} = 143.99°$, λ(Cu Kα) = 154.06 pm, $T = 100$ K, 13 538 reflections, 2036 unique reflections ($R_{int.} = 0.0439$, $R_\sigma = 0.0266$), multi-scan absorption correction ($\mu = 16.0$ mm^{-1}, SADABS-2016/2),[28] structure solution with olex2.solve,[29] full-matrix-least-squares refinement on |F^2|, anisotropic refinement for all atoms (SHELXL),[30] $R_1 = 0.0267$, $wR_2 = 0.0872$ for 2036 reflections with $I \geq 2\sigma(I)$ and $R_1 = 0.0273$, $wR_2 = 0.0875$ for all 13 538 reflections, max./min. residual electron density = 0.90/−1.82 e$^-$/Å^3.

Pd[B(S_2O_7)$_2$]$_2$-II: blue octahedra (0.271 × 0.188 × 0.184 mm), tetragonal, $P4_1$, $Z = 8$, $a = 13.8210(5)$ Å, $b = 13.8210(5)$ Å, $c = 21.724(1)$ Å, $V = 4149.7(4)$ Å^3, $\rho = 2.66$ g·cm^{-3}, $2\theta_{max} = 56°$, λ(Mo Kα) = 71.073 pm, $T = 100$ K, 237 806 reflections, 9995 unique reflections ($R_{int.} = 0.0359$, $R_\sigma = 0.0117$), multi-scan absorption correction ($\mu = 1.8$ mm^{-1}, SADABS-2016/2),[28] structure solution with SHELXT,[31] full-matrix-least-squares refinement on |F^2|, anisotropic refinement for all atoms atoms (SHELXL),[30] $R_1 = 0.0224$, $wR_2 = 0.0583$ for 9995 reflections with $I > 2\sigma(I)$ and $R_1 = 0.0224$, $wR_2 = 0.0583$ for all reflections, max./min. residual electron density = 0.97/−0.85 e$^-$/Å^3. The structure was refined as an inversion twin of a meroedric twin with the twin matrices (0 1 0, 1 0 0, 0 0 -1) and (-1 0 0, 0 -1 0, 0 0 -1) and a domain ratio of 0.52(3); 0.04(1); 0.40(2); 0.05(1)).

Pd[B(SO_4)(S_2O_7)]: red cubic plates (0.127 × 0.066 × 0.043 mm), monoclinic, $P2_1/c$, $Z = 2$, $a = 6.7061(2)$ Å, $b = 16.0198(4)$ Å, $c = 8.1681(2)$ Å, $\beta = 94.923(1)°$, $V = 874.27(4)$Å^3, $\rho = 2.55$ g·cm^{-3}, $2\theta_{max} = 68.63°$, λ(Mo Kα) = 71.073 pm, $T = 100$ K, 34 955 reflections, 3353 unique reflections ($R_{int.} = 0.0542$, $R_\sigma = 0.0340$), multi-scan absorption correction ($\mu = 1.9$ cm^{-1}, SADABS-2016/2),[28] structure solution with olex2.solve,[29] full-matrix-least-squares refinement on |F^2|, anisotropic refinement for all atoms (SHELXL),[30] $R_1 = 0.0429$, $wR_2 = 0.1205$ for 3353 reflections with $I > 2\sigma(I)$ and $R_1 = 0.0553$, $wR_2 = 0.1275$ for all 34 955 reflections, max./min. residual electron density = 1.58/−2.01 e$^-$/Å^3.

Deposition Numbers 2 443 731 (for Pd[B(S_2O_7)$_2$]$_2$-I), 244 732 (for Pd[B(S_2O_7)$_2$]$_2$-II) and 244 733 (for Pd[B(SO_4)(S_2O_7)]$_2$) contain the supplementary crystallographic data for this paper. These data are provided free of charge by the joint Cambridge Crystallographic Data Centre and Fachinformationszentrum Karlsruhe Access Structures service.

Powder X-ray diffraction (P-XRD) and Rietveld refinement

P-XRD data were collected on a Stoe Stadi-P powder diffractometer with a Mythen detector and a Debye − Scherrer geometry by using Mo-$K_{\alpha 1}$ radiation of $\lambda = 0.70930$ Å. The samples were ground and sealed in glass capillaries with 0.5 mm diameter. The data was recorded in a range of $2\theta = 0$–60° within 480 minutes. The Rietveld refinement was performed with Topas, refining the lattice parameters freely using the Thompson-Cox-Hastings profile function.[32] The background was described with six Chebyshev polynomials. The diffractogram was plotted using Origin software.[32]

Physical property measurements: Crystals of the two polymorphs of Pd[B(S_2O_7)$_2$]$_2$ were carefully crushed between two slides into a rough powder and filled into polypropylene capsules. The samples were attached to the sample holder of a Dynacool physical properties measurement system (PPMS) by Quantum Design and measured using the vibrating sample magnetometer (VSM) option. They were investigated in a temperature range of 2–300 K and at applied external fields up to 90 kOe. Fitting and plotting the data was done with Origin software[33] and the graphical editing with the program CorelDraw 2024.[34]

Infrared spectroscopy: The sample characterization was conducted using a Bruker Optics Alpha IR spectrometer. Measurements were performed at room temperature utilizing a diamond ATR module, with a maximum spectral resolution of 1 cm^{-1}. Data analysis and visualization were carried out using Origin software.[32]

Acknowledgments

We thank Dr. Jörg Neudörfl for the collection and the evaluation of the X-ray data of Pd[B(S_2O_7)$_2$]$_2$-I. The work was funded by the Deutsche Forschungsgemeinschaft (DFG, German Research Foundation) – 528508733 and INST 211/1034–1. Markus Suta gratefully acknowledges a scholarship of the "Young College" of the North-Rhine Westphalian Academy of Sciences, Humanities, and the Arts.

Open access funding enabled and organized by Projekt DEAL.

Conflict of Interest

The authors declare no conflict of interest.

Data Availability Statement

The data that support the findings of this study are available in the supplementary material of this article.

Keywords: borosulfate · crystal structure · magnetochemistry · palladium · solvothermal synthesis

[1] H. A. Höppe, K. Kazmierczak, M. D. K. Förg, F. Fuchs, H. Hillebrecht, *Angew. Chem., Int. Ed.* **2012**, *51*, 6255; *Angew. Chem.* **2012**, *124*, 6359.
[2] J. Bruns, H. A. Höppe, M. Daub, H. Hillebrecht, H. Huppertz, *Chem. Eur. J.* **2020**, *26*, 7966.
[3] a) L. Kang, X. Liu, Z. Lin, B. Huang, *Phys. Rev. B* **2020**, *102*, 205424; b) Y. Li, Z. Zhou, S. Zhao, F. Liang, Q. Ding, J. Sun, Z. Lin, M. Hong, J. Luo, *Angew. Chem., Int. Ed.* **2021**, *60*, 11457.
[4] a) M. D. Ward, B. L. Chaloux, M. D. Johannes, A. Epshteyn, *Adv. Mater.* **2020**, *32*, 2003667; b) B. L. Chaloux, J. A. Ridenour, M. D. Johannes, A. Epshteyn, *Adv. Energy Sustainability Res.* **2022**, *3*, 2200029.
[5] a) L. M. Träger, L. C. Pasqualini, H. Huppertz, J. Bruns, M. Suta, *Angew. Chem., Int. Ed.* **2023**, *62*, e202309212; Angew. Chem. 2023, 135, e202309212; b) P. Netzsch, M. Hämmer, P. Gross, H. Bariss, T. Block, L. Heletta, R. Pöttgen, J. Bruns, H. Huppertz, H. A. Höppe, *Dalton Trans.* **2019**, *48*, 4387; c) P. Netzsch, F. Pielnhofer, R. Glaum, H. A. Höppe, *Chem. Eur. J.* **2020**, *26*, 14745; d) P. Netzsch, P. Gross, H. Takahashi, H. A. Höppe, *Inorg. Chem.* **2018**, *57*, 8530.
[6] P. Netzsch, R. Stroh, F. Pielnhofer, I. Krossing, H. A. Höppe, *Angew. Chem., Int. Ed.* **2021**, *60*, 10643; *Angew. Chem*. **2021**, *133*, 10738.
[7] L. C. Pasqualini, H. Huppertz, M. Je, H. Choi, J. Bruns, *Angew. Chem., Int. Ed.* **2021**, *60*, 19740; *Angew. Chem.* **2021**, *133*, 19892.
[8] D. van Gerven, S. Sutorius, J. Bruns, M. S. Wickleder, *ChemistryOpen* **2022**, *11*, e202200122.
[9] S. Sutorius, D. van Gerven, S. Olthof, B. Rasche, J. Bruns, *Chem. Eur. J.* **2022**, *28*, e202200004.
[10] J. Bruns, D. van Gerven, T. Klüner, M. S. Wickleder, *Angew. Chem., Int. Ed.* **2016**, *55*, 8121; *Angew. Chem.* **2016**, *128*, 8253.
[11] J. Waser, H. A. Levy, S. W. Peterson, *Acta Crystallogr.* **1953**, *6*, 661.
[12] J. Bruns, T. Klüner, M. S. Wickleder, *Chem. Eur. J.* **2015**, *21*, 1294.
[13] T. Dahmen, P. Rittner, S. Boeger-Seidl, R. Gruehn, *J. Alloys Compd.* **1994**, *216*, 11.
[14] a) N. Bartlett, R. Maitland, *Acta Crystallogr.* **1958**, *11*, 747; b) A. Tressaud, J. L. Soubeyroux, H. Touhara, G. Demazeau, F. Langlais, *Mater. Res. Bull.* **1981**, *16*, 207; c) B. Bachmann, B. G. Müller, *Z. Anorg. Allg. Chem.* **1993**, *619*, 387; d) B. G. Müller, *J. Fluorine Chem.* **1982**, *20*, 291; e) B. Bachmann, B. G. Müller, *Z. Anorg. Allg. Chem.* **1993**, *619*, 189; f) N. Ruchaud, J. Grannec, A. Tressaud, G. Férey, *Z. Anorg. Allg. Chem.* **1995**, *621*, 1958; g) H. Bialowons, B. G. Müller, *Z. Anorg. Allg. Chem.* **1997**, *623*, 434; h) M. Müller, B. G. Müller, *Z. Anorg. Allg. Chem.* **1995**, *621*, 1385; i) E. Alter, R. Hoppe, *Z. Anorg. Allg. Chem.* **1974**, *408*, 115.
[15] Z. M. Fu, W. X. Li, *Sci. China Ser. A.* **1996**, *39*, 981.
[16] D. Orosel, M. Jansen, *Z. Anorg. Allg. Chem.* **2006**, *632*, 1131.
[17] N. V. Izarova, M. H. Dickman, R. Ngo Biboum, B. Keita, L. Nadjo, V. Ramachandran, N. S. Dalal, U. Kortz, *Inorg. Chem.* **2009**, *48*, 7504.
[18] J. Bruns, M. Eul, R. Pöttgen, M. S. Wickleder, *Angew. Chem., Int. Ed.* **2012**, *51*, 2204; *Angew. Chem*. **2012**, *124*, 2247.
[19] J. Bruns, O. Niehaus, R. Pöttgen, M. S. Wickleder, *Chem. Eur. J.* **2014**, *20*, 811.
[20] P. Netzsch, H. A. Höppe, *Eur. J. Inorg. Chem.* **2021**, *11*, 1065.
[21] J. Bruns, T. Klüner, M. S. Wickleder, *Angew. Chem., Int. Ed.* **2013**, *52*, 2590; *Angew. Chem.* **2013**, *125*, 2650.
[22] M. Daub, K. Kazmierczak, H. A. Höppe, H. Hillebrecht, *Chem. Eur. J.* **2013**, *19*, 16954.
[23] H. Lueken, *Magnetochemie*. B. G. Teubner: Stuttgart, Leipzig, Chapter 2.2, **1999**.
[24] N. Ruchaud, J. Grannec, A. Tressaud, *J. Alloys Compd.* **1994**, *205*, 17.
[25] U. Oetliker, H.-U. Güdel, *J. Lumin.* **1993**, *58*, 350.
[26] D. Paus, R. Hoppe, *Z. Anorg. Allg. Chem.* **1977**, *431*, 207.
[27] a) D. Reinen, *Struct. Bond.* **1969**, *6*, 30; b) J. Ferguson, K. Knox, D. L. Wood, *J. Chem. Phys.* **1961**, *35*, 2236.
[28] G. M. Sheldrick, *SADABS, Empirical Absorption corrections program*, University of Göttingen **1995**.
[29] O. V. Dolomanov, L. J. Bourhis, R. J. Gildea, J. A. K. Howard, H. Puschmann, *J. Appl. Crystallogr.* **2009**, *42*, 339.
[30] G. M. Sheldrick, *Acta Crystallogr. Sect. C.* **2015**, *71*, 3.
[31] G. M. Sheldrick, *Acta Crystallogr. Sect. A: Found. Crystallogr.* **2015**, *71*, 3.
[32] OriginPro 2024 (version 10.1.0.170), OriginLab Corporation, Nothhampton, Massachusetts (USA), **2024**.
[33] a) A. A. Coelho, *J. Appl. Crystallogr.* **2018**, *51*, 210; b) Topas-Academic (version V6), Brisbane (Australia), **2016**.
[34] *CorelDRAW Graphics Suite* p. 2017 (version 19.0.0.328), Corel Corporation: Ottawa, Ontario (Canada), **2017**.

Manuscript received: April 22, 2025
Revised manuscript received: May 30, 2025
Version of record online: June 27, 2025